

Study on the mechanism of nitrogen conversion in NH₃-doped methane premixed flame based on multi-spectral analysis methods

Gangfu Rao^{a,b}, Meirong Dong^{a,b,*}, Wei Nie^c, Xiao Lin^{a,b}, Youcai Liang^{a,b}, Jidong Lu^{a,b}

^a School of Electric Power, South China University of Technology, Guangzhou, Guangdong, 510640, China

^b Guangdong Province Engineering Research Center of High Efficient and Low Pollution Energy Conversion, Guangzhou, Guangdong, 510640, China

^c Anhui Institute of Optics and Fine Mechanics, Hefei Institutes of Physical Sciences, Chinese Academy of Sciences, Hefei, 230031, China

ARTICLE INFO

Handling Editor: Dr. Paul Williams

Keywords:

Nitrogen conversion

Image spectroscopy

Tunable diode laser absorption spectroscopy

Plane laser-induced fluorescence

ABSTRACT

It is essential to obtain the in-situ key radicals and components in the combustion process of NH₃ oxidation to reveal the volatile nitrogen conversion mechanism. In this work, multi-spectral analysis methods, including image spectroscopy, Tunable diode laser absorption spectroscopy (TDLAS), and plane laser-induced fluorescence (PLIF) were used to obtain the spatial distribution characteristics of the main excited radicals (C₂^{*}/CH^{*}/CN^{*}/OH^{*}), H₂O, and NO in NH₃-doped methane flames, respectively. Furthermore, the kinetic simulation was combined to obtain the key reactions and main pathways of nitrogen conversion. The experimental results showed that when the concentration of NH₃ was low, the NO generated in lean flame was less than that in rich flame, which was more than that in rich flame when the concentration of NH₃ was high. NH₃ also promoted the formation of H₂O in flames. The image spectral intensity of CN^{*} had a significant linear relationship with the CN concentration obtained by simulation, indicating that CN^{*} was mainly generated by CN thermal excitation. The results of sensitivity and path analysis indicated that rich flame contributed to the reaction of N-species with H and that high NH₃ concentration promoted the conversion of NH₂ to HNO. With increasing NH₃ concentration and equivalence ratio, the proportion of CH₃ conversion to C₂H₆ was enhanced, while the proportion of CH₃ oxidized decreased. This work reveals the mechanism of volatile nitrogen (NH₃) conversion and the influence of equivalence ratio and NH₃ concentration on it, which provides theoretical guidance for NO_x emission reduction.

1. Introduction

Nitrogen oxides (NO_x) produced by fuel combustion are responsible for environmental safety problems such as acid rain and photochemical pollution. According to the different sources of nitrogen, NO_x is divided into thermal NO_x, prompt NO_x, and fuel NO_x. Fuel NO_x contributes the most to the formation of NO_x during solid fuel combustion. Volatile nitrogen is an important source of fuel NO_x. Especially in biomass fuels, the proportion of volatile nitrogen in total nitrogen could reach more than 80 % [1,2]. NH₃ is the main volatile nitrogen released during the combustion of low-rank coal and biomass [3]. Therefore, it is a key step to reveal the oxidation process of NH₃ in constructing the mechanism of nitrogen conversion network.

The composition of solid fuel is complex and there are diverse factors affecting nitrogen conversion. Therefore, it is difficult to obtain a widely applicable nitrogen conversion mechanism directly using solid fuel as the research object. It is a feasible scheme to obtain the conversion

mechanism of volatile nitrogen by studying the flame doped with NH₃. Alves et al. [4] found that the conversion yield of NH₃ to NO decreased with the increase of NH₃ in low-concentration NH₃ (500–2000 ppm) doped methane premixed flame. Slefarski et al. [5] discovered that in the CH₄/NH₃ co-combustion flame, with the increase of NH₃ concentration, the concentration of NO generated increased slowly. Especially at the equivalence ratio of 0.95, the NO production was almost unchanged with the increase of NH₃. According to the numerical simulation results, Sullivan et al. [6] claimed that the main reason for the slow growth of NO production with the increase of NH₃ in low concentration NH₃ (0~1000 ppm) doped flame was the reduction reaction between NO and NH_i. As an important parameter of combustion, the effect of the equivalence ratio on NH₃ oxidation is also worth considering. Li et al. [7] analyzed the effect of equivalence ratio on the oxidation of NH₃ by detecting the NO production in the NH₃-doped methane premixed flames. The results showed that with the increase of equivalence ratio (0.65–1.45), the production of NO increased first and then decreased,

* Corresponding author. School of Electric Power, South China University of Technology, Guangzhou, Guangdong, 510640, China.

E-mail address: epdongmr@scut.edu.cn (M. Dong).

<https://doi.org/10.1016/j.joei.2023.101437>

Received 27 August 2023; Received in revised form 18 October 2023; Accepted 18 October 2023

Available online 19 October 2023

1743-9671/© 2023 Published by Elsevier Ltd on behalf of Energy Institute.

and the production of NO was highest at an equivalence ratio of 1.0. Shmakov et al. [8] also found that the concentration of NO generated in rich flame was lower than that in equivalent and lean flame based on molecular beam mass spectrometry (MBMS). But Sun et al. [9] obtained different conclusions by detecting the formation of NO in volatile nitrogen. They believed that at the same temperature, the volatile-N conversion ratio increased with the increase of excess oxygen ratio (0.6–1.4).

In the above studies, researchers had focused on the direct analysis of the effect of NH₃ on NO_x, and less on the intermediate components and their influence mechanism on the oxidation of NH₃. Nitrogen conversion is composed of a series of complex reactions, so obtaining information of intermediate components is a prerequisite for clarifying the role of each component in the fulcrum of the nitrogen transformation network. Therefore, it is necessary to carry out the detection and analysis of key intermediate radicals in the nitrogen conversion.

As a non-invasive detection technology, optical detection technology could realize high-precision in-situ detection of components information in combustion diagnostics. Different optical detection technologies have different emphases on the detection object due to their different technical principles. **Image spectroscopy is mainly applied to detect OH*/CH*/C₂*/CN*** and other excited radicals with strong spontaneous emission signals in flames [10–14]. Laser-induced fluorescence (LIF) is mainly used to detect OH, CH, NO, and other radicals in flame [15–22]. Tunable diode laser absorption spectroscopy (TDLAS) could achieve high-precision detection of H₂O, CH₄, CO₂, and other components [23–28]. It is a feasible approach to obtain information of on intermediate components and products in the NH₃ oxidation by using multi-spectral analysis methods, to realize the analysis of the whole process of nitrogen conversion (source-intermediate component-product).

In this work, NH₃ was added to the CH₄ premixed flat flame to analyze the nitrogen conversion in flame. The spatial distribution characteristics of the main excited radicals (C₂*/CH*/CN*/OH*), the main nitrogen products (NO), and the main combustion products (H₂O) in the flame were obtained by image spectroscopy, PLIF, and TDLAS, respectively. The experimental and simulation results based on different kinetic mechanisms were further compared to optimize the kinetic model suitable for the oxidation of NH₃. Finally, sensitivity analysis and ROP analysis were performed using the optimized kinetic mechanism to reveal the mechanism of NH₃ concentration and equivalence ratio on nitrogen conversion.

2. Methods and experimental

2.1. Experiment setup

NH₃ is the main component of volatile nitrogen, and the concentrations of NH₃ released by different fuels in the devolatilization stage is different. Biomass with high nitrogen content such as corn straw can release NH₃ concentrations up to 1500 ppm [29], while coal usually releases less. Therefore, the adding concentrations of NH₃ were set as

0–1500 ppm in the CH₄ premixed flame.

The multi-optical gas flame detection platform consists of an optical detection section and a gas supply section, which was represented in Fig. 1 (a and b), respectively. Premixed flat one-dimensional flames were established over a water-cooled stainless steel porous-plug McKenna-type burner (Holthuis & Associates) with a diameter of 60 mm. The central stream consisted of CH₄, N₂, O₂, and NH₃ which were supplied from high-purity gas cylinders (99.9% stated purity). The equivalence ratio of flame was set to 0.8/1.0/1.1 to analyze the effect of the equivalence ratio on NH₃ oxidation. The gas flows shown in Table 1 were accurately controlled by mass flow meters. Meanwhile, the shroud flow of N₂ was kept at 2 L/min to reduce the influence of the atmosphere on the flame. The burner was mounted on a translation stage to allow accurate translation of the flame relative to the optical measurement components.

The optical detection section was composed of image spectroscopy, PLIF, and TDLAS device. The excited radical spontaneous emission was obtained by ICCD (DH734, Andor, 1024 × 1024 pixels) coupled with the filter. The central wavelengths of the filters for capturing CH*, CN*, C₂*, and OH* were 434 nm, 390 nm, 514.5 nm, and 315 nm, respectively. The bandwidth filter (FGUV11) was used to reduce the interference of yellow-green light on the spontaneous emission of OH*. The average value of 20 spectra was selected as the analysis data to reduce the influence of random error. The PLIF device consisted of a 10 Hz Nd:YAG laser (Spectra Physics Quanta-Ray, 10 ns/pulse) coupled with a dye laser. A laser sheet was used to produce about 50 mm height and 0.1 mm thickness light for flame diagnosis, as in the same system by Wang et al. [30]. The NO excitation wavelength (225.84 nm) was chosen to receive a strong signal when scanning the laser wavelength, and pulse energy was around 0.3 mJ. The fluorescence signal was collected by an ICCD (IRO, 1024 × 1024 pixels) equipped with an achromatic UV lens (105 mm, f/4.5) and filter. The gain and gate times were set to 95 ns and 55 ns, respectively. For each flame, 200 images were collected and the sum of all images was used as the analysis data. The wavelength scanning-direct absorption TDLAS device was mainly composed of the function generator, laser drive, DFB laser, laser detector, and data acquisition card. The absorption signal of H₂O near 7185 cm⁻¹ and 7444 cm⁻¹ was used in this work. The calculation method of H₂O concentration based on TDLAS technology was the same as that of So et al. [25]. The mean value of 35 spectra was used as the analysis data of TDLAS. During measurement, the laser outlet and laser detector were located close to the burner to reduce the influence of the atmosphere on the detection, and the laser passed through the center of the flame.

Table 1

The flow rates of gases.

Equivalence ratio (φ)	CH ₄ (L/min)	O ₂ (L/min)	N ₂ (L/min)	NH ₃ concentration (ppm)
0.8	1.466	3.665	13.799	0/500/800/1000/
1.0	1.809	3.618	13.503	1200/1500
1.1	1.965	3.275	13.690	

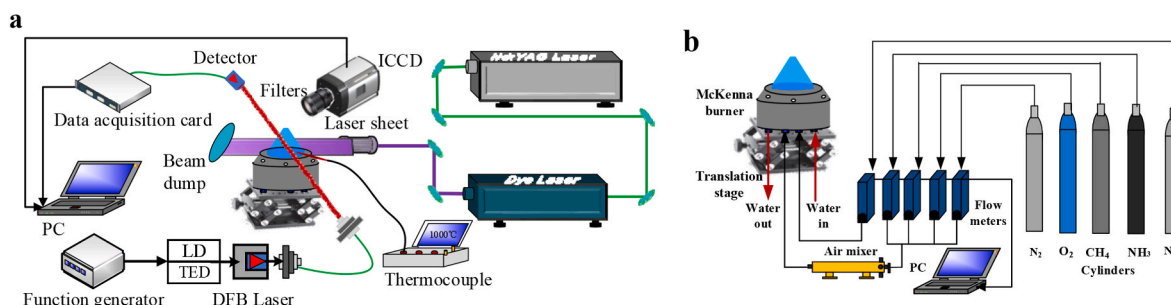


Fig. 1. Schematic diagram of multi-optical gas flame detection platform: (a) multi-optical detection section; (b) gas section.

2.2. Kinetic modeling

Sensitivity analysis, and rate of production (ROP) analysis were modeled relying on a detailed kinetic database using the Premixed Laminar Flame-Speed Calculation program from the Chemkin PRO package. The parameters GRAD = 0.02 and CURV = 0.02 resulted in a grid of ~650 points. The kinetic models of nitrogen conversion proposed by Okafor et al. [31] and Glarborg et al. [32] were shown to be reliable over a wide range of NH₃ concentrations and equivalence ratios, which was applied in this work. The production and consumption reactions of the excited radicals were displayed in Table 2. The reactions of C₂ were the same as in Smith et al. [33].

3. Results and discussion

3.1. Spatial distribution characteristics of excited radicals based on image spectroscopy

Radical is an important characterization substance in the intermediate process of nitrogen conversion. The spontaneous emission of the main excited radicals (OH*/CH*/C₂*/CN*) in the flame can be captured by image spectroscopy to analyze the effect of NH₃ on the formation and transformation of radicals. OH* and CH* are often used to characterize flamelet [37], which reflects the main combustion reaction zone and is also involved in nitrogen conversion. CN* is an important intermediate N-species in nitrogen conversion. C₂* is an important characterization of hydrocarbon conversion. Fig. 2 shows the spatial distribution of excited radicals in a methane flame with 1000 ppm NH₃ added.

The distribution areas of the spontaneous emission of the excited radicals are similar, and they are mainly distributed in the area 2–4 mm from the nozzle, which is the central reaction zone of the combustion. Compared to the other three radicals, the main distribution area of OH* is closer to the nozzle, especially in lean flames. The spatial distribution of CH*, CN*, and C₂* is similar in flames. OH* is mainly generated by CH + O₂=OH*+CO. The generation paths of CH* are C₂H + O=CH*+CO and C₂H + O₂=CH*+CO₂. CH₂+C=C₂*+H is the main generation reaction of C₂*. The main generation area of OH* is closer to the nozzle, indicating that CH was generated earlier than C₂H. The dehydrogenation of CH₂ gradually generates CH and C, so CH is generated later than CH₂ and C is generated later than CH, resulting in the OH* distribution area being closer to the nozzle compared to C₂*. The effect of NH₃ concentration on the spatial distribution of radicals is relatively small. As shown in Fig. 3, the spatial distribution of CN* changes with the increase of NH₃ concentration in flame.

The maximum radiation intensity of excited radicals at different NH₃ concentrations was further compared to obtain the effect of NH₃ on the formation and transformation of radicals. The experimental results were compared with the maximum concentration of excited radicals predicted by the simulation. The results are shown in Figs. 4–7.

In the lean flame, the spectral intensity of C₂* increases with NH₃

concentration; in the equivalent and rich flames, it decreases with increasing of NH₃, which is consistent with the simulation results based on the Okafor mechanism. The kinetic simulation results based on the Glarborg mechanism show that the C₂* concentration decreases with the increase of NH₃ in the equivalent and rich flame, and the trend is not obvious in the lean flame. C₂* is mainly generated by C + CH₂=C₂*+H₂. Compared to the Okafor mechanism, the Glarborg mechanism contains more C_xH_yO_z and N-species. CH_i would react with these components or transform to produce them, resulting in a more complex reaction pathway. In addition, the reactions between CH_i and N-species are weaker in the lean flame, which leads to the inconspicuous trend of C₂* concentration predicted by the Glarborg mechanism with the increase of NH₃. The simulation results based on the Okafor mechanism with less CH_i reactions predict that CH₂ and C would increase with the increase of NH₃ concentration in lean flame, which leads to the increase of C₂* with the increase of NH₃ concentration. It can be found that both experimental and simulation results show that C₂* increases with increasing equivalence ratio. Especially in the rich flame, the C₂* production increases rapidly. The spectral intensity of CH* increases with NH₃ in lean and equivalent flame. In the rich flame, the spectral intensity of CH* decreases with NH₃. The trend of the simulated CH* mole fraction with NH₃ based on the Okafor mechanism is similar to the experimental results. The simulation results based on the Glarborg mechanism show that the CH* decreases with NH₃ in the equivalent and rich flame, and the trend is not obvious in the lean flame. The formation paths of CH* are C₂H + O=CH*+CO and C₂H + O=CH*+CO₂. Based on the Glarborg mechanism with more CH_i reactions, the formation and conversion paths of C₂H are more complicated, and the increase of NH₃ has little effect on C₂H in lean and equivalent flames. In lean flame, the increase of NH₃ leads to little change of O₂/O concentration. With the increase of equivalence ratio, the increase of NH₃ leads to the decrease of O₂/O, which leads to the decrease of CH* with the increase of NH₃ based on Glarborg mechanism simulation in equivalent flame. Based on the Okafor mechanism with less CH_i reaction, C₂H increases with the increase of NH₃, resulting in the increase of CH* with the increase of NH₃ in lean and equivalent flames.

The OH* decreases with the increase of NH₃, indicating that NH₃ inhibits the formation of OH*. The spectral intensity of CN* increases with NH₃, and the simulation results also show that the mole of CN increases with NH₃. To reveal the relationship between CN* and CN, the function fitting of CN* spectral intensity and simulated CN mole fraction was carried out. The results are presented in Table 3.

The fitting results show that the correlation coefficient R² between the simulated mole fraction of CN and the spectral intensity of CN* in three equivalence ratio flames reaches 0.99, indicating that there is a significant linear relationship between them. It is well known that there are two main ways to generate excited radicals: chemical excitation and thermal excitation [38]. The strong linear relationship between CN* and CN indicates that CN* is mainly produced by CN thermal excitation.

3.2. Spatial distribution characteristics of NO based on PLIF

The relationship between the fluorescence signal intensity (S_F(t)) and the initial population of the probed initial state (N_i⁰) is shown in Eq. (1) [10].

$$S_F(t) = hv \frac{\Omega}{4\pi} \epsilon l A N_i^0 b_{if} A_{fi} \tau_{laser} \times e^{-\frac{t}{\tau_{eff}}} \quad (1)$$

where h represents Planck's constant; ν is the fluorescence wave-number; Ω is the solid angle for detection, ϵ is the detector efficiency, l is the probe volume length, A is the probe volume cross-section area, b_{if} is the rate coefficient for absorption transitions between states i and f , A_{fi} is the Einstein coefficient for spontaneous emission, τ_{laser} is the laser pulse duration, and τ_{eff} is the effective fluorescence lifetime.

It can be seen from Eq. (1) that the initial population of the probed initial state is positively correlated with the fluorescence signal

Table 2

The production and consumption mechanism of excited radicals.

Excited radicals	Production	Collisional quenching	Spontaneous emission
OH*	CH + O ₂ =OH*+CO [33] O + H + M=OH*+M [33] OH + OH + H=OH*+H ₂ O [34]	OH*+M = OH + M [35]	OH* = OH [35]
CH*	C ₂ H + O=CH*+CO [34] C ₂ H + O ₂ =CH*+CO ₂ [34]	CH*+M = CH + M [35]	CH* = CH [35]
C ₂ *	C + CH ₂ =C ₂ *+H ₂ [36]	C ₂ *+M = OH + M [33]	C ₂ * = C ₂ [33]

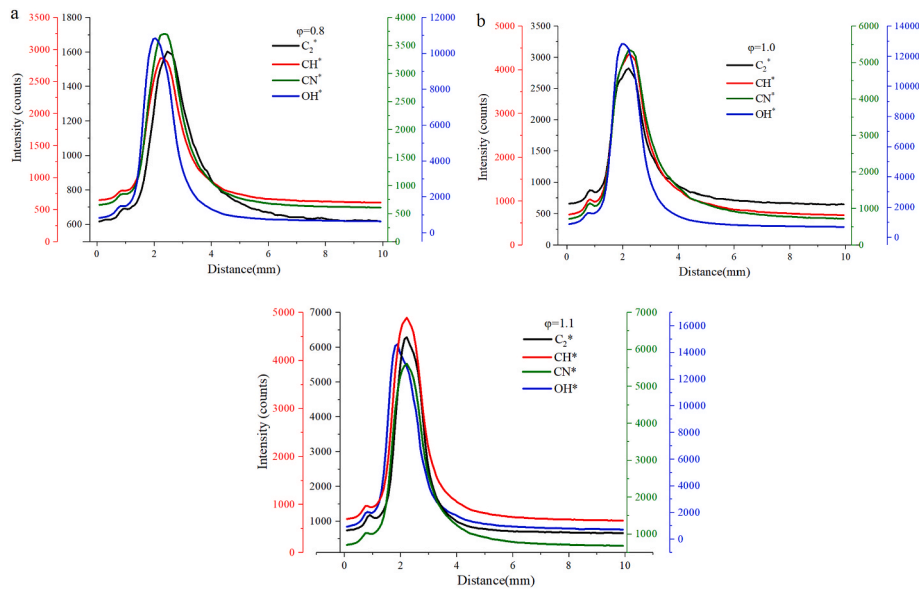


Fig. 2. Spatial distribution of excited radicals in flames of different equivalence ratios: (a) $\phi = 0.8$; (b) $\phi = 1.0$; (c) $\phi = 1.1$.

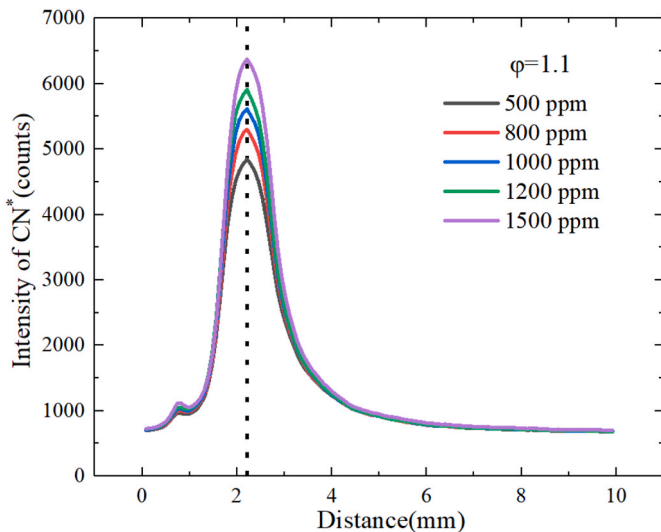


Fig. 3. The spatial distribution of CN^* changes with the increase of NH_3 concentration in the rich flame.

intensity, that is, the fluorescence signal intensity could be used to qualitatively reflect the concentration of the substances to be measured. The cumulative results of 200 images taken by the ICCD are shown in Fig. 8. NO is distributed throughout the flame. The image obtained by the ICCD is the accumulation on the line of sight. Therefore, in order to obtain the spatial distribution characteristics of NO, the mean value of NO-PLIF intensity at 1 mm near the central axis of the flame is calculated and analyzed, as shown in Fig. 9. The intensity of NO-PLIF increases rapidly to the maximum near the nozzle, then decreases and remains relatively stable, and decreases finally. The decrease in fluorescence intensity after the first peak may be caused by atmospheric diffusion into the flame. The fluorescence signals in the relatively stable region (20–25 mm from the nozzle) were selected and used to analyze the effect of NH_3 addition on NO formation, as shown in Fig. 10.

As shown in Fig. 10(a), the intensity of NO-PLIF increases with the increase of NH_3 concentration, and its growth rate slows down, indicating that the conversion rate of NO generated by NH_3 oxidation decreases with the increase of NH_3 concentration. Sullivan et al. [39]

found the same results in the detection of NO concentration in ammonia-doped methane flame flue gas, which is mainly due to the increase of NO reduction reaction with the increase of NH_3 concentration. The intensity of NO-PLIF in the equivalent flame is greater than that of the other two flames, reflecting that the most NO is generated during combustion at the equivalent ratio. When the NH_3 concentration is low, more NO is produced in the rich flame than in the lean flame, whereas when the NH_3 concentration is high, more NO is produced in the lean flame. These trends are also reflected in the simulation results based on the Okafor and Glarborg mechanisms, suggesting that both mechanisms models can reflect the changing trend of NO with initial NH_3 concentration.

3.3. Effect of NH_3 on H_2O based on TDLAS

As the main product of combustion, the change in H_2O concentration reflects the effect of nitrogen conversion on combustion. From the experimental results of image spectroscopy, it can be seen that the combustion reaction zone is mainly in the area of 2–4 mm from the nozzle, so the position of 5 mm from the nozzle is selected as the detection position of TDLAS. The spectrum obtained directly by TDLAS was the transmission signals of lasers with wavenumber near 7185 cm^{-1} and 7444 cm^{-1} absorbed by H_2O , as shown in Fig. 11. According to Beer-Lambert law, spectral absorbance (α_v) and laser intensity (I) have a functional relationship as shown in Eq. (2).

$$\alpha_v = -\ln\left(\frac{I_t}{I_0}\right) \quad (2)$$

where I_0 represents the incident laser intensity; I_t is laser intensity transmitted through a homogeneous gas medium.

The concentration of the target component (x_{abs}) on the absorption path can be calculated using Eq. (3).

$$x_{abs} = \frac{A}{LPS(T)} \quad (3)$$

where A represents the integrated absorbance of the gas, which can be obtained by processing the transmission signal of the absorption spectrum; L is the absorption path length; P is the absorbing species pressure; $S(T)$ is the temperature-dependent strength of the line.

The gas temperature can be calculated using the double-line method, and the results are shown in Fig. 12. The temperature of the lean flame is lower than that of the rich and equivalent flame. $S(T)$ is further obtained

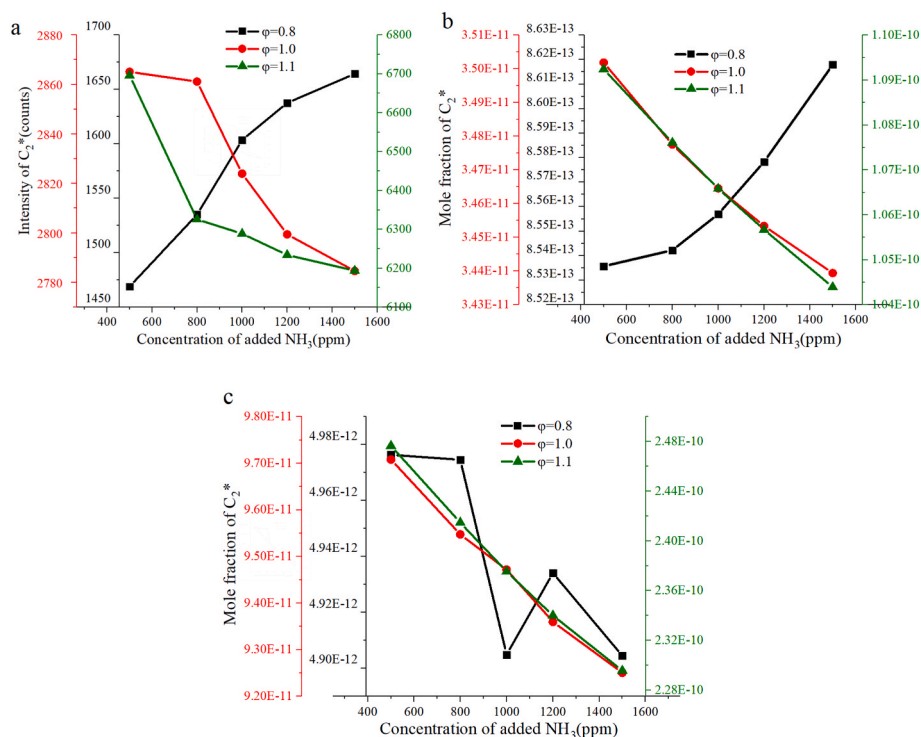


Fig. 4. Spectral intensity of C_2^* and simulated calculation concentration at different NH_3 concentrations: (a) spectral intensity; (b) simulation results based on Okafor mechanism; (c) simulation results based on Glarborg mechanism.

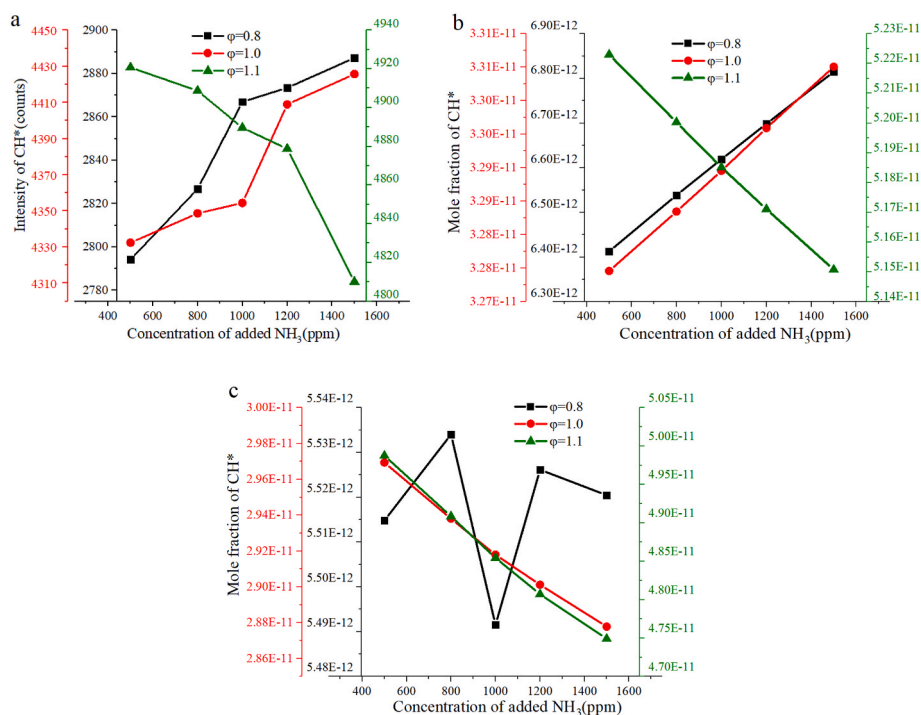


Fig. 5. Spectral intensity of CH^* and simulated calculation concentration at different NH_3 concentrations: (a) spectral intensity; (b) simulation results based on Okafor mechanism; (c) simulation results based on Glarborg mechanism.

according to the temperature results, and the H_2O concentration can be further calculated using Eq. (3). The predicted final H_2O concentration is shown in Fig. 13. The experimental results demonstrate that the concentration of H_2O increases with the increase of initial NH_3 concentration in the three equivalence ratio flames. With the increase of the equivalence ratio, the concentration of H_2O increases, which is

consistent with the results of simulation predictions. According to the law of atomic conservation, H from NH_3 is eventually converted to H_2O , so the increase of NH_3 would lead to the increase of H_2O . In the flames with equivalence ratios of 0.8, 1.0, and 1.1, the maximum relative errors of H_2O concentration obtained by experiment and predicted by simulation are 7%, 4%, and 2%, respectively, indicating that both

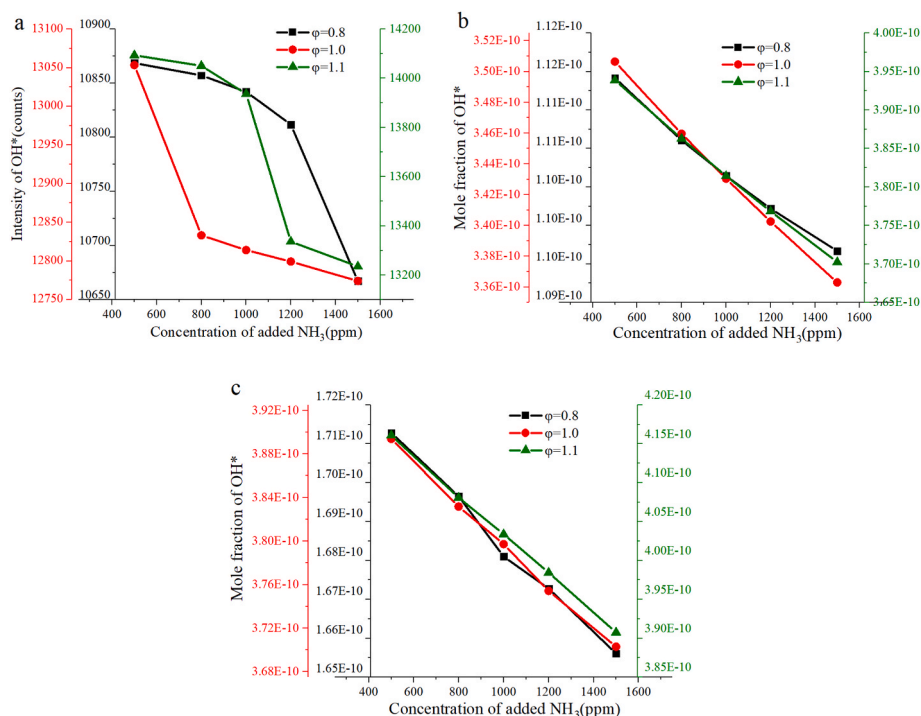


Fig. 6. Spectral intensity of OH^* and simulated calculation concentration at different NH_3 concentrations: (a) spectral intensity; (b) simulation results based on Okafor mechanism; (c) simulation results based on Glarborg mechanism.

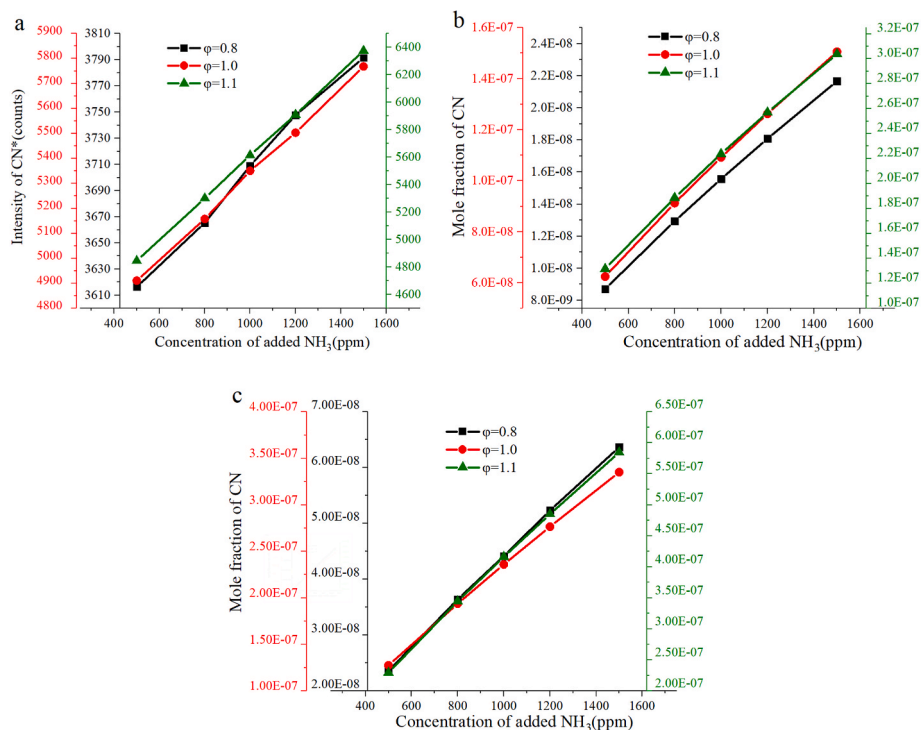


Fig. 7. Spectral intensity of CN^* (a) and simulated CN concentration at different NH_3 concentrations: (b) simulation results based on Okafor mechanism; (c) simulation results based on Glarborg mechanism.

mechanisms could reflect the formation of H_2O . The results of H_2O concentration detection show that the addition of NH_3 would have a certain effect on the main reaction of combustion.

3.4. NH_3 oxidation pathway analysis

Compared with the Glarborg mechanism, the simulation results based on the Okafor mechanism are more consistent with the experimental results. This suggests that the Okafor mechanism could better describe how NH_3 is converted at low concentrations. Therefore, the

Table 3
Fitting results of CN* spectral intensity and simulated CN mole fraction.

ϕ	Results (Okafor)		Results (Glarborg)	
	Functions	R ²	Functions	R ²
0.8	$y = -2.48 \times 10^{-7} + 7.10 \times 10^{-11}x$	0.99	$y = -7.72 \times 10^{-7} + 2.20 \times 10^{-10}x$	0.99
1.0	$y = -4.39 \times 10^{-7} + 1.02 \times 10^{-10}x$	0.99	$y = -1.06 \times 10^{-6} + 2.42 \times 10^{-10}x$	0.99
1.1	$y = -3.97 \times 10^{-7} + 1.10 \times 10^{-10}x$	0.99	$y = -8.72 \times 10^{-7} + 2.29 \times 10^{-10}x$	0.99

Okafor mechanism was used to analyze the sensitivity of the main product NO to obtain the main reactions and key radicals that play a critical role in the production and transformation of NO. The results are presented in Fig. 14.

The reactions that play an important role in promoting NO formation mainly include the production reaction of OH/O ($H + O_2 = O + OH$), the

oxidation reaction of N-species, and the production reaction of CO/CO₂. $H + O_2 = O + OH$ has the most significant promoting effect on NO formation. The reaction is the main production reaction of oxidizing radical OH/O, and the production of NO is derived from the oxidation of N-species, so it is essential for the production of NO. The production of NO is also promoted by $NH_2 + O = HNO + H$ and $NH + O = NO + H$. As the increase of equivalence ratio, the promoting effect of $N + O_2 = NO + O$ on NO production is gradually enhanced.

The reactions that have important inhibitory effects on the production of NO mainly include the NO reduction reaction, the reaction between CH_i and NO, the mutual conversion reaction of CH₄ and CH₃, and the HO₂ production reaction. In lean flame, $H + O_2 + H_2O = HO_2 + H_2O$ has the strongest inhibitory effect on NO production. NO is oxidized to NO₂ by the reaction $NO + HO_2 = NO_2 + OH$. Therefore, it is feasible to inhibit the formation of NO by the reaction of HO₂ formation. In the equivalent and rich flames, the production of NO is more inhibited by $H + CH_3 (+M) = CH_4 (+M)$. As the initial reaction of combustion, the dehydrogenation reaction of CH₄ controls the subsequent reactions. This

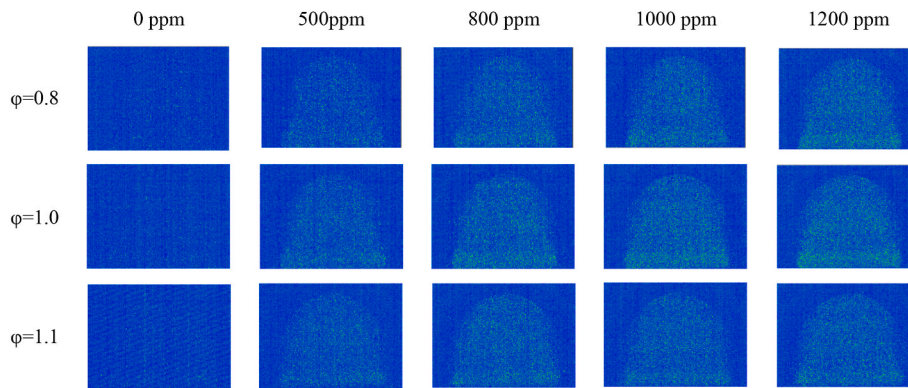


Fig. 8. The NO-PLIF image of flames captured by ICCD.

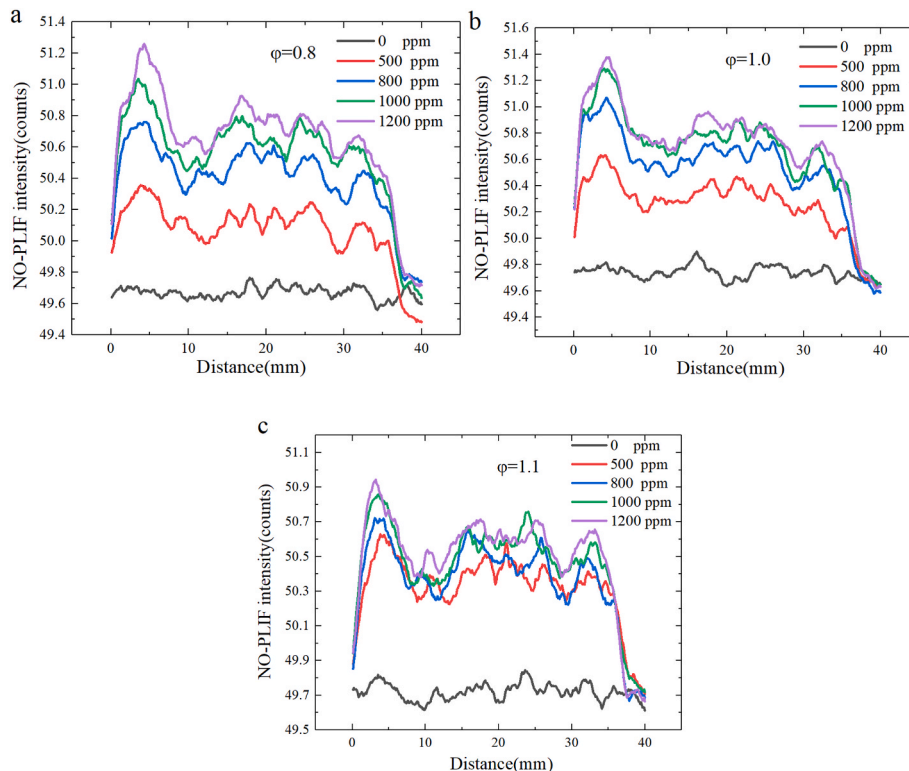


Fig. 9. Spatial distribution of fluorescence intensity near the central axis:(a) $\phi = 0.8$; (b) $\phi = 1.0$; (c) $\phi = 1.1$.

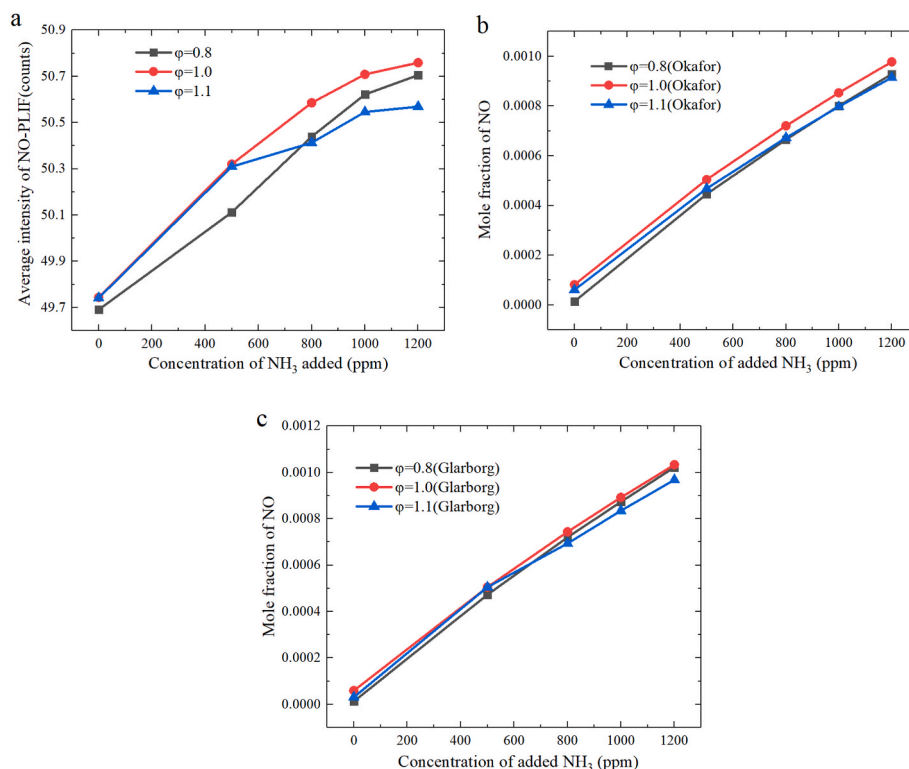


Fig. 10. Comparison of NO-PLIF intensity and simulated predicted NO concentration: (a) NO-PLIF intensity; (b) simulated concentration based on Okafor; (c) simulated concentration based on Glarborg.

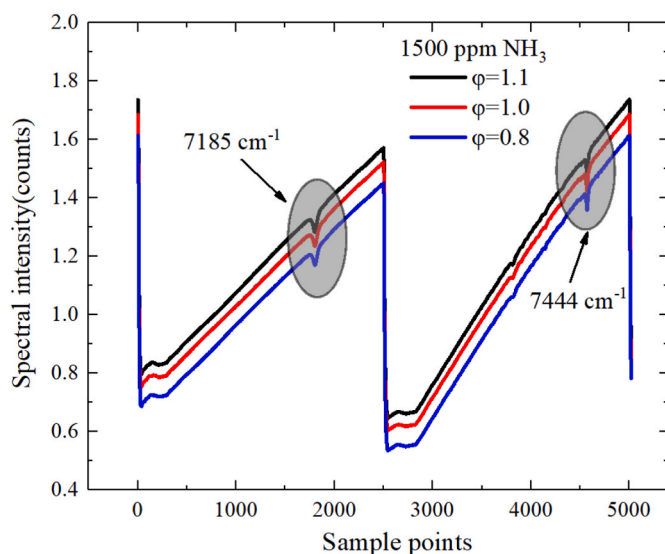


Fig. 11. Original absorption spectra of H₂O based on TDLAS.

reaction causes CH₃ to regenerate CH₄, which inhibits combustion. The formation of NO relies on the combustion reaction to provide oxidizing groups, so it also has an important inhibiting effect on the production of NO. In the three equivalence ratio flames, NH + NO = N₂O + H has a large negative sensitivity coefficient. In the lean flame, NH₂ + NO = N₂ + H₂O also inhibits the production of NO. In the equivalent and rich flames, N + NO = N₂ + O has a more significant inhibiting effect on the production of NO. The inhibiting effect of CH₂ + NO = H + HCO on NO production is noteworthy in the equivalent and rich flame, and the effect in the rich flame is stronger than that in the equivalent flames. The reduction reaction of NO is the main way for the reduction

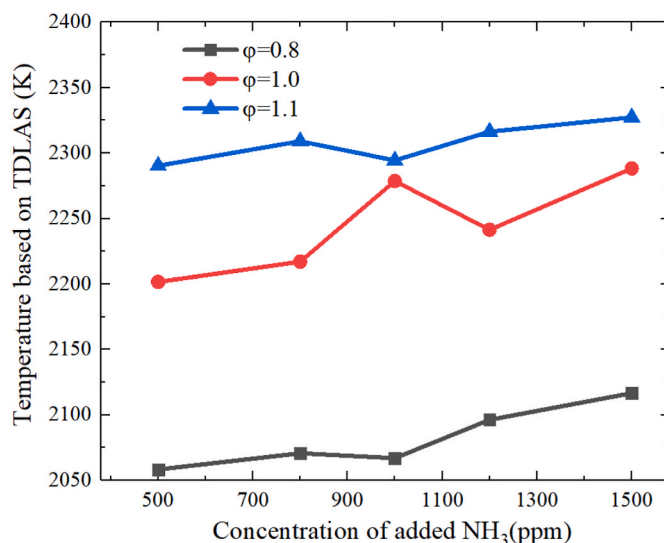


Fig. 12. Gas temperature obtained by TDLAS.

of NO emissions. Therefore, it was further compared that the ROP of the main NO reduction reaction in different flames. The results are exhibited in Fig. 15.

In the three equivalence ratio flames, the reaction rates of all NO reduction reactions increase with the increase of NH₃ concentration. It can be seen that NH₂ + NO = N₂ + H₂O is an important NO reduction path, and the reaction rate decreases as the equivalence ratio increases, while NH₂ + NO = NNH + OH has a similar tendency. When less NH₃ is added, the reaction rate of NH + NO = N₂O + H is the fastest in the rich flame, followed by the equivalent flame, and slowest in the lean flame. When more NH₃ is added, the rate of this reaction is accelerated with the

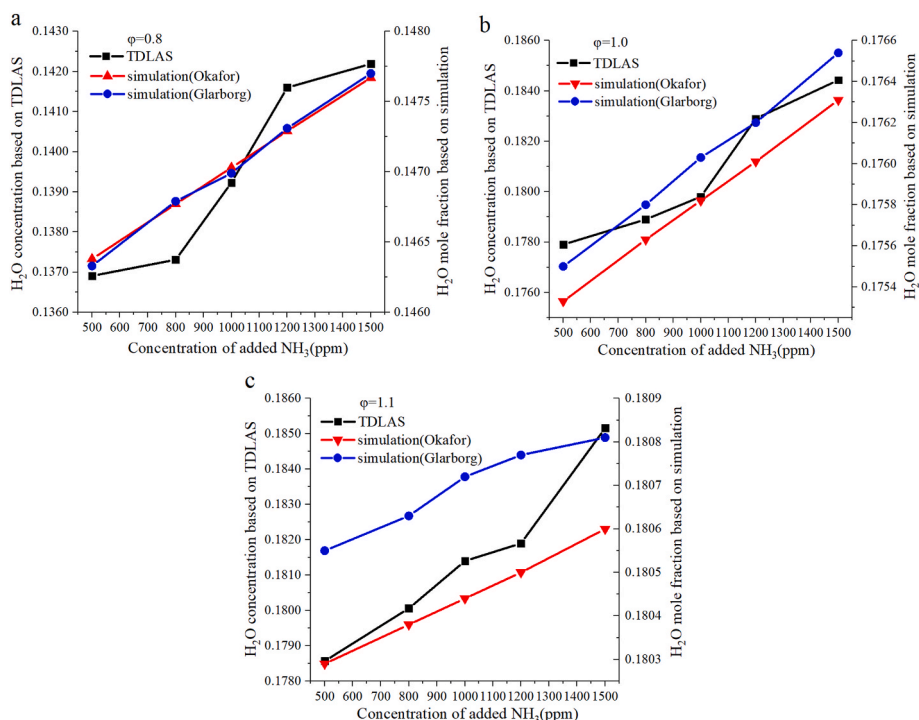


Fig. 13. Comparison of H₂O concentration obtained by TDLAS and simulation: (a) $\phi = 0.8$; (b) $\phi = 1.0$; (C) $\phi = 1.1$.

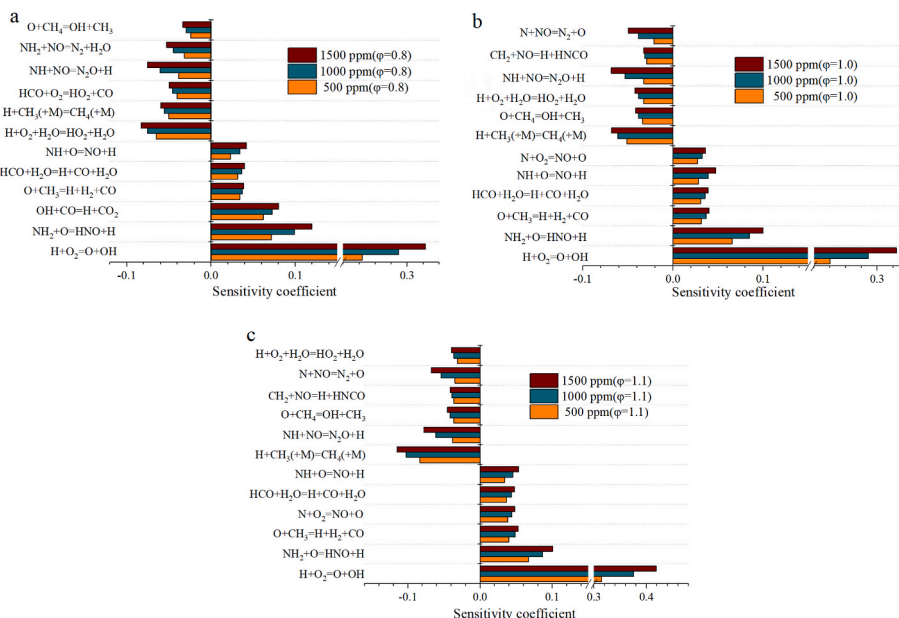


Fig. 14. Results of NO sensitivity analysis at different equivalence ratios based on Okafor: (a) $\phi = 0.8$; (b) $\phi = 1.0$; (c) $\phi = 1.1$.

increase of the equivalence ratio. $N + NO = N_2 + O$ shows a similar trend to this reaction. It should be noted that the rate of $N + NO = N_2 + O$ increases rapidly with the increase of equivalence ratio when higher amounts of NH_3 are added. Based on the above analysis, it can be concluded that when the concentration of NH_3 is low, the produced NO is lower in the lean flame due to the faster reaction rate of $NH_2 + NO = N_2 + H_2O$. With the increase of NH_3 concentration, the rate of $N + NO = N_2 + O$ increases rapidly with the increase of equivalence ratio in the rich flame, resulting in a lower NO concentration.

Through the ROP analysis of NO, it was obtained that the direct effects of NH_3 concentration and equivalence ratio on the reaction of NO

formation or consumption. The oxidation process of NH_3 and the role of intermediate groups in nitrogen conversion still need to be analyzed by constructing a nitrogen conversion path network. Therefore, the full computational domain ROP analysis based on the Okafor mechanism was performed on the main nitrogen-containing components involved in the nitrogen conversion and the results are presented in Fig. 16. The number shown in the diagram is the proportion (ϕ_{A-B}) of reactant A consumed in the i_{th} reaction in all consumed reactions of A, and its calculation method is shown in Eq. (4).

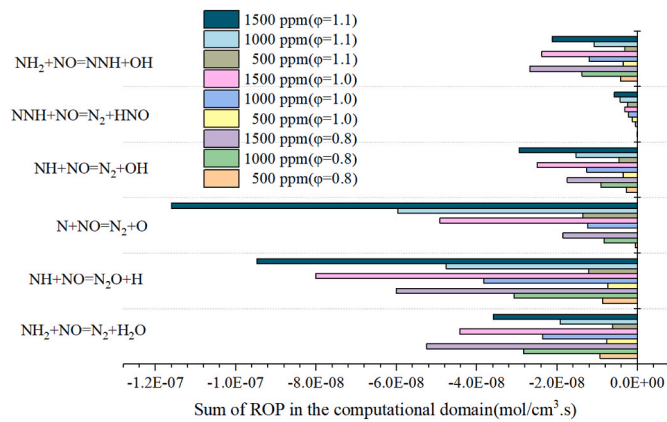


Fig. 15. The sum of ROP of NO reduction reactions in the computational domain.

$$\varphi_{A-B}^i = \frac{\int_0^L ROP_i^j dl}{\sum_i^n \left(\int_0^L ROP_i^j dl \right)} \times 100\% \quad (4)$$

where $\int_0^L ROP_i^j dl$ is the ROP integral value of the i_{th} reaction in the computational domain; $\sum_i^n \left(\int_0^L ROP_i^j dl \right)$ is the sum of ROP integrals of all reactions that consume reactant A.

The oxidation process of NH_3 involves multiple reaction paths and various intermediate radicals. Firstly, NH_3 would be converted to NH_2 , and $NH_3 + OH = NH_2 + H_2O$ is the main reaction pathway. NH_2 reacts with H/O/OH to generate NH or reacts with O to produce HNO. Among them, $NH_2 + O = HNO + H$ accounts for the largest proportion in the lean flame {Sullivan, 2002 #286} {Sullivan, 2002 #286} {Sullivan, 2002 #286}. HNO is further oxidized to NO, among which HNO tends to react with H. NH is oxidized by O to NO, or dehydrogenation to N. Some NH also reacts with OH to form HNO. In the lean flame, NH tends to react with O, whereas, in the rich flame, the reaction between NH and H is dominant. Most of the N is converted to NO, and a small amount of N also undergoes a series of reactions to form other intermediate N-species such as HCN/CN/NCO. As the NH_3 concentration increases, the proportion of N-species oxidation reactions decreases, especially the conversion of NH_2 to HNO.

NO also reacts with other radicals while it is produced. The main conversion paths of NO are as follows: (1) NO is further oxidized to NO_2 ; (2) NO regenerates HNO; (3) NO reacts with CH_i ; (4) the reduction reaction of NO with intermediate N-species. There is a strong equilibrium between NO and NO_2 in the flame. The increase of equivalence ratio and NH_3 would inhibit the conversion of NO to NO_2 . Increasing the

equivalence ratio helps to promote path (2), while NH_3 reduces the proportion of this path. $NO + CH_2 = HNCO + H$ is the largest proportion in the path (3). Most of the HNCO reacts with H to generate NH_2 , and a small proportion would also be converted to NCO. NO would also react with CH to form N or HCN. Increasing the equivalence ratio has a catalytic effect on the path (3), and NH_3 has a small impact on it. Path (4) consists of two sub-pathways, the first path is $NO - N_2O - NO$, and the other path is $NO - N_2$. The effect of the equivalence ratio on the path (4) can be concluded as follows: it inhibits the reaction of NO with NH_2 , promotes the reaction of NO with N, and has little effect on the reaction of NO with NH. NH_3 has a positive effect on all NO reduction reactions, and the promoting effect increases with NH_3 , which leads to the phenomenon that the conversion rate of NH_3 to NO decreases with NH_3 .

3.5. Effect of NH_3 on the main combustion reactions

According to the NO sensitivity analysis and the nitrogen reaction path network, carbon-containing components play an important role in nitrogen conversion, especially CH_i , whose formation and conversion depend on the main combustion reaction. The involvement of carbon-containing components in nitrogen conversion would lead to a change in their concentration, which would have some impact on the main combustion reaction. Therefore, studying the effect of NH_3 on the main combustion reaction is a key step to revealing the coupling effect of nitrogen conversion and the main combustion reaction. The full computational domain ROP analysis of the main combustion reactions was performed based on the Okafor mechanism, as shown in Fig. 17.

The reaction paths of CH_4 mainly include: (1) CH_4 is dehydrogenated to CH_3 . CH_3 is further oxidized to generate CH_2O/CH_3OH and finally CO and CO_2 , as shown in the blue arrow. $CH_4 - CH_3 - CH_2O - HCO - CO - CO_2$ is the main pathway of the CH_4 reaction; (2) CH_4 is gradually converted into CH_3 , $CH_2(S)$, and CH_2 by dehydrogenation reaction and further oxidized to CO/ CO_2 , as shown in the green arrow; (3) CH_4 is gradually dehydrogenated and converted to CH_2/CH , which is further oxidized to CH_2O and HCO, and finally converted to CO and CO_2 , as shown in the red arrow; (4) two CH_3 radicals are combined to form C_2H_6 , which is gradually dehydrogenated and finally converted to CO and CO_2 , as shown in the black arrow; (5) CH_3 reacts with H to regenerate CH_4 , as shown in the brown arrow.

Fig. 17 (a and b) show that the increase in equivalence ratio would inhibit CH_3 is oxidized to CH_2O and dehydrogenated to $CH_2(S)$, while it would promote the reaction of CH_3 to produce C_2H_6 . It is noteworthy that the increase in equivalence ratio would promote the conversion of CH_3 to CH_2 . It can be seen that the increase in the equivalence ratio also has a positive effect on the reaction of CH_3 to CH_4 . It is attributed to the relative decrease in the concentration of oxidizing radicals as the equivalence ratio increases, which leads to a weakening CH_i oxidation reaction. Therefore, unoxidized CH_3 would be regenerated to CH_4 or converted to higher hydrocarbons. It can be also noticed from Fig. 17(c and d) that the proportion of CH_4 reaction path (1) and (3) decreases with the increase of NH_3 , while the proportion of path (4) increases.

The production path of C_2^* is $CH_2 + C = C_2^* + H_2$. It can be seen from Fig. 17(ád) that the main path of CH_2 production is $CH_4 - CH_3 - CH_2(S) - CH_2$. In the lean flame, the proportion of this path increases with the

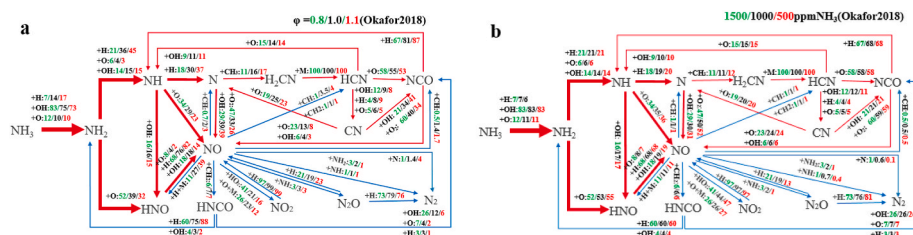


Fig. 16. NH_3 oxidation path diagram: (a) different equivalence ratios (1500 ppm NH_3); (b) different NH_3 concentrations ($\varphi = 0.8$).

Funding information

The research was supported by National Natural Science Foundation of China [No. 51976064] and [No. 62105104].

Declaration of competing interest

The authors declare that they have no known competing financial interests or personal relationships that could have appeared to influence the work reported in this paper.

Acknowledgement

The research was supported by National Natural Science Foundation of China (No. 51976064/No. 62105104), Guangdong Basic and Applied Basic Research Foundation (2022A151010709). We also acknowledge the support from the Fundamental Research Funds for the Central Universities (2022ZFJH04) and Guangdong Province Key Laboratory of Efficient and Clean Energy Utilization (2013A061401005).

References

- [1] J. Riaza, P. Mason, J.M. Jones, J. Gibbins, H. Chalmers, High temperature volatile yield and nitrogen partitioning during pyrolysis of coal and biomass fuels, *Fuel* 248 (7) (2019) 215–220.
- [2] P. Abelha, S. Leiser, J.R. Pels, M.K. Cieplik, Combustion properties of upgraded alternative biomasses by washing and steam explosion for complete coal replacement in coal-designed power plant applications, *Energy* 248 (6) (2022), 123546.
- [3] P. Glarborg, Fuel nitrogen conversion in solid fuel fired systems, *Prog. Energy Combust. Sci.* 29 (2) (2003) 89–113.
- [4] M. Alves, C. Rosa, M. Costa, Effect of the oxidizer composition on the CO and NO_x emissions from a laboratory combustor operating under oxy-fuel conditions, *Energy Fuels* 27 (1) (2013) 561–567.
- [5] R. Slefarski, P. Czyzewski, M. Golebiewski, Experimental study on combustion of CH₄/NH₃ fuel blends in an industrial furnace operated in flameless conditions, *Therm. Sci.* 24 (6A) (2020) 3625–3635.
- [6] N. Sullivan, A. Jensen, P. Glarborg, M.S. Day, J.F. Grcar, J.B. Bell, Ammonia conversion and NO_x formation in laminar coflowing nonpremixed methane-air flames, *Combust. Flame* 131 (3) (2002) 285–298.
- [7] B. Li, Y. He, Z. Li, A.A. Konnov, Measurements of NO concentration in NH₃-doped CH₄+Air flames using saturated laser-induced fluorescence and probe sampling, *Combust. Flame* 160 (1) (2013) 40–46.
- [8] A.G. Shmakov, O.P. Korobeinichev, I.V. Rybitskaya, A.A. Chernov, D.A. Knyazkov, T.A. Bolshova, A.A. Konnov, Formation and consumption of NO in H₂+O₂+N₂ flames doped with NO or NH₃ at atmospheric pressure, *Combust. Flame* 157 (3) (2010) 556–565.
- [9] S. Sun, H. Cao, H. Chen, X. Wang, J. Qian, T. Wall, Experimental study of influence of temperature on fuel-N conversion and recycle NO reduction in oxyfuel combustion, *Proc. Combust. Inst.* 33 (2) (2011) 1731–1738.
- [10] D. Alviso, M. Mendieta, J. Molina, J.C. Rolón, Flame imaging reconstruction method using high resolution spectral data of OH*, CH* and C₂* radicals, *Int. J. Therm. Sci.* 121 (11) (2017) 228–236.
- [11] C. Hu, Y. Gong, Q. Guo, X. Song, G. Yu, An experimental study on the spectroscopic characteristics in coal-water slurry diffusion flames based on hot-oxygen burner technology, *Fuel Process. Technol.* 154 (12) (2016) 168–177.
- [12] C. Moon, Y. Sung, S. Ahn, T. Kim, G. Choi, D. Kim, Thermochemical and combustion behaviors of coals of different ranks and their blends for pulverized-coal combustion, *Appl. Therm. Eng.* 54 (1) (2013) 111–119.
- [13] S.L. Sheehe, S.I. Jackson, Spatial distribution of spectrally emitting species in a nitromethane-air diffusion flame and Comparison with kinetic models, *Combust. Flame* 213 (3) (2020) 184–193.
- [14] T. Zhang, Q. Guo, Q. Liang, Z. Dai, G. Yu, Distribution characteristics of OH*, CH*, and C₂* luminescence in CH₄/O₂ Co-flow diffusion flames, *Energy Fuels* 26 (9) (2012) 5503–5508.
- [15] C. Brackmann, J. Bood, J.D. Naucclér, A.A. Konnov, M. Aldén, Quantitative picosecond laser-induced fluorescence measurements of nitric oxide in flames, *Proc. Combust. Inst.* 36 (3) (2017) 4533–4540.
- [16] C. Brackmann, E.J.K. Nilsson, J.D. Naucclér, M. Aldén, A.A. Konnov, Formation of NO and NH in NH₃-doped CH₄ + N₂ + O₂ flame: experiments and modelling, *combust. Flame* 194 (8) (2018) 278–284.
- [17] C. Brackmann, B. Zhou, Z.S. Li, M. Aldén, Strategies for quantitative planar laser-induced fluorescence of NH radicals in flames, *Combust. Sci. Technol.* 188 (4–5) (2016) 529–541.
- [18] L. Jiang, C. Gu, G. Zhou, F. Li, Q. Wang, Cellular instabilities of N-Butane/Air flat flames probing by PLIF-OH and PLIF-CH₂O laser diagnosis, *Exp. Therm. Fluid Sci.* 118 (10) (2020), 110155.
- [19] C.M. Mitsingas, S.D. Hammack, E.K. Mayhew, R. Rajasegar, B. McGann, A. W. Skiba, C.D. Carter, T. Lee, Simultaneous high speed PIV and CH PLIF using R-branch excitation in the C²σ⁺-x2π (0,0) band, *Proc. Combust. Inst.* 37 (2) (2019) 1479–1487.
- [20] A.R. Qubbaj, Laser-induced fluorescence measurements in venturi cascaded propane gas jet flames, *J. Energy Inst.* 83 (2) (2010) 114–123.
- [21] B. Zhou, C. Brackmann, Z. Li, M. Aldén, Development and application of CN PLIF for single-shot imaging in turbulent flames, *Combust. Flame* 162 (2) (2015) 368–374.
- [22] Y. Zhou, Z. Wang, Y. He, R. Whiddon, D. Xu, Z. Li, K. Cen, Effects of CH₄ content on NO formation in one-dimensional adiabatic flames investigated by saturated laser-induced fluorescence and CHEMKIN modeling, *Energy Fuels* 31 (3) (2017) 3154–3163.
- [23] T. Kamimoto, Y. Deguchi, Y. Kiyota, High temperature field application of two dimensional temperature measurement technology using CT tunable diode laser absorption spectroscopy, *Flow Meas. Instrum.* 46 (12) (2015) 51–57.
- [24] Z. Yao, W. Zhang, M. Wang, J. Chen, Y. Shen, Y. Wei, X. Yu, F. Li, H. Zeng, Tunable diode laser absorption spectroscopy measurements of high-pressure ammonium dinitramide combustion, *Aero. Sci. Technol.* 45 (9) (2015) 140–149.
- [25] S. So, J. Park, M. Yoo, J. Hwang, D. Kim, C. Lee, Simultaneous measurement of OH radical, H₂O concentration, and temperature in a premixed CH₄/air flame using TDLAS with an improved analysis method, *Opt Express* 30 (18) (2022) 32031–32050.
- [26] X. Lin, M. Dong, W. Nie, G. Rao, J. Lu, Time-to-Frequency conversion method for tunable diode laser absorption spectrum, *Optik* 270 (11) (2022), 170049.
- [27] G.Y. Zhang, G.Q. Wang, Y. Huang, Y.Z. Wang, X.C. Liu, Reconstruction and simulation of temperature and CO₂ concentration in an axisymmetric flame based on TDLAS, *Optik* 170 (2018) 166–177.
- [28] W. Nie, Z. Xu, G. Rao, X. Lin, J. Lu, M. Dong, R. Kan, Methods of tunable diode laser absorption saturation spectroscopy to gas sensing under optically thick conditions, *Microw. Opt. Technol. Lett.* 63 (8) (2021) 2063–2067.
- [29] A. Anca-Couce, P. Sommersacher, N. Evic, R. Mehrabian, R. Scharler, Experiments and modelling of NO_x precursors release (NH₃ and HCN) in fixed-bed biomass combustion conditions, *Fuel* 222 (6) (2018) 529–537.
- [30] Q. Wang, L. Jiang, W. Cai, Y. Wu, Study of UV Rayleigh scattering thermometry for flame temperature field measurement, *J. Opt. Soc. Am. B* 36 (10) (2019) 2843–2849.
- [31] E.C. Okafor, Y. Naito, S. Colson, A. Ichikawa, T. Kudo, A. Hayakawa, H. Kobayashi, Experimental and numerical study of the laminar burning velocity of CH₄-NH₃-air premixed flames, *Combust. Flame* 187 (1) (2018) 185–198.
- [32] T. Mendiara, P. Glarborg, Ammonia chemistry in oxy-fuel combustion of methane, *Combust. Flame* 156 (10) (2009) 1937–1949.
- [33] G.P. Smith, J. Luque, C. Park, J.B. Jeffries, D.R. Crosley, Low pressure flame determinations of rate constants for OH(A) and CH(A) chemiluminescence, *Combust. Flame* 131 (1–2) (2002) 59–69.
- [34] G.P. Smith, C. Park, J.A. Luque, Note on chemiluminescence in low-pressure hydrogen and methane-nitrous oxide flames, *Combust. Flame* 140 (4) (2005) 385–389.
- [35] M. Tamura, P.A. Berg, J.E. Harrington, J. Luque, J.B. Jeffries, G.P. Smith, D. R. Crosley, Collisional quenching of CH(A), OH(A), and NO(A) in low pressure hydrocarbon flames, *Combust. Flame* 114 (3–4) (1998) 502–514.
- [36] J. Grebe, K.H. Homann, Blue-green chemiluminescence in the system C₂H₂/O/H. Formation of the emitters CH(A²Δ), C₂(d³Πg) and C₂H*, *Ber. Bunsenges. Phys. Chem.* 86 (7) (1982) 587–597.
- [37] W. Weng, M. Costa, Z. Li, M. Aldén, Temporally and spectrally resolved images of single burning pulverized wheat straw particles, *Fuel* 224 (7) (2018) 434–441.
- [38] M.D. Leo, A. Saveliev, L. Kennedy, S. Zelepouga, OH and CH luminescence in opposed flow methane oxy-flames, *Combust. Flame* 149 (4) (2007) 435–447.
- [39] N. Sullivan, J. Anker, P. Glarborg, M.S. Day, J.F. Grcar, J.B. Bell, C.J. Pose, R. J. Kee, Ammonia conversion and NO_x formation in laminar coflowing nonpremixed methane-air flames, *Combust. Flame* 131 (3) (2002) 285–298.